Analytical and Bioanalytical Chemistry (2020) 412:691–702
https://doi.org/10.1007/s00216-019-02279-y

RESEARCH PAPER

Development of methodology to generate, measure, and characterize the chemical composition of oxidized mercury nanoparticles

Avik J. Ghoshdastidar[1] · Janani Ramamurthy[1] · Maxwell Morissette[1] · Parisa A. Ariya[1,2]

Received: 12 April 2019 / Revised: 9 November 2019 / Accepted: 12 November 2019 / Published online: 18 December 2019

Abstract

The phase of oxidized mercury is critical in the fate, transformation, and bioavailability of mercury species in Earth's ecosystem. There is now evidence that what is measured as gaseous oxidized mercury (GOM) is not only gaseous but also consists of airborne nanoparticles with distinct physicochemical properties. Herein, we present the development of the first method for the consistent and reproducible generation of oxidized mercury nano- and sub-micron particles (~ 5 to 400 nm). Oxidized mercury nanoparticles are generated using two methods, vapor-phase condensation and aqueous nebulization, for three proxies: mercury(II) bromide ($HgBr_2$), mercury(II) chloride ($HgCl_2$), and mercury(II) oxide (HgO). These aerosols are characterized using scanning mobility and optical sizing, high-resolution scanning transmission electron microscopy (STEM), and nano/microparticle interface coupled to soft ionization mercury mass spectrometric techniques. Synthetic nanoparticle stability was studied in aqueous media, and using a microcosm at ambient tropospheric conditions of ~ 740 Torr pressure, room temperature, and at relative humidity of approximately 20%. Analysis of microcosm airborne nanoparticles confirmed that generated synthetic mercury nanoparticles retain their physical properties once in air. KCl-coated denuders, which are currently used globally to measure gaseous mercury compounds, were exposed to generated oxidized mercury nanoparticles. The degree of synthetic mercury nanoparticle capture by KCl-coated denuders and particulate filters was assessed. A significant portion of nanoparticulate and sub-micron particulate mercury was trapped on the KCl-coated denuder and measured as GOM. Finally, we demonstrate the applicability of soft ionization mercury mass spectrometry to the measurement of mercury species present in the gaseous and solid phase. We recommend coupling of this technique with existing methodology for a more accurate representation of mercury biogeochemistry cycling.

Keywords Gaseous oxidized mercury (GOM) · KCl-coated denuders · Particulate-bound mercury (PBM) · Mercury mass spectrometry

Introduction

Atmospheric mercury is characterized by three bulk, operationally defined species: gaseous elemental mercury (Hg^0), gaseous oxidized mercury (GOM), and particulate-bound mercury (PBM) [1]. Hg^0 is the predominant species in the atmosphere and is measured using preconcentration on gold traps, thermal desorption followed by cold-vapor atomic fluorescence spectroscopy (CVAFS), cold vapor atomic absorption spectroscopy (CVAAS), or inductively coupled plasma mass spectrometry (ICP-MS). It is by far the most abundant mercury species in the atmosphere with concentrations in the low ng/m^3 range in urban areas [2, 3].

Gaseous oxidized mercury (GOM), generally regarded as Hg^{2+} species, has been detected in both tropospheric and stratospheric air at pg/m^3 concentrations. GOM is measured by trapping to KCl-coated denuders, followed by thermal decomposition and measurement as Hg^0. Until recently, the

Electronic supplementary material The online version of this article (https://doi.org/10.1007/s00216-019-02279-y) contains supplementary material, which is available to authorized users.

✉ Parisa A. Ariya
parisa.ariya@mcgill.ca

[1] Department of Chemistry, McGill University, 801 Sherbrooke St. West, Montreal H3A 2K6, Canada

[2] Department of Atmospheric and Oceanic Sciences, McGill University, 805 Sherbrooke St. West, Montreal H3A 0B9, Canada

chemical identity of gaseous oxidized mercury was largely unknown though mercury mass spectrometry has confirmed the detection of $HgBr_2$ and $HgCl_2$ in urban air [4]. GOM is generally more reactive and more water-soluble than Hg^0, which promotes absorption into rain droplets, deposition to terrestrial and aquatic environments, and scavenging from the atmosphere [5].

KCl-coated denuders were developed in the 1990s as a technique for measuring oxidized mercury species and involve the conversion of oxidized mercury species to a $HgCl_4^{2-}$ species incorporated into the potassium chloride coating [6]. At 600 °C, this species is thermally decomposed and reduced, producing gaseous Hg^0, which is measured using cold-vapor atomic fluorescence spectroscopy. In addition to differences in the efficiencies by which distinct gaseous oxidized mercury species are trapped, KCl-coated denuder trapping efficiencies and GOM release are affected by the presence of ozone [7, 8]. It has also been shown that humidity can passivate the KCl surface, causing GOM to be underestimated; at varying humidities, the KCl-coated denuder surface does not behave consistently in its trapping of oxidized mercury species [7–9]. Placing a KCl-coated denuder upstream of PBM filters reduces a significant positive artifact caused by GOM adsorbing to the filter [10]; however, in the presence of high ozone concentration, a preceding denuder increases downstream PBM concentrations [11]. Despite these complications, KCl-coated denuders continue to be used as they allow for more straightforward analytical procedures and higher-time resolution measurements.

Conventional methodologies of studying atmospheric mercury are limited to determining whether mercury is elemental, inorganic, or particulate but fail to give the actual chemical species present. Gaseous oxidized mercury has long been suspected to be mercuric (Hg^{2+}) species such as HgO [12, 13], $HgCl_2$ [14], $HgBr_2$ [15], $Hg(OH)_2$ [15], $HgSO_4$, $Hg(NO_2)_2$ [16], or mixed halogen species [17]. Evidence for stable Hg^{1+} has also been found, such as HgBr from the oxidation of Hg^0 with BrO radicals [18]. $HgCl_2$ and $HgBr_2$ were indirectly identified in field samples via thermo-desorption profiles for nylon exchange membranes [9] and more recently directly in Montreal urban air, by nano/microparticle adsorption interface preconcentration atmospheric pressure chemical ionization mass spectrometry or particle-trap mercury mass spectrometry [4]. Mercury mass spectrometry (Hg-MS) involves the trapping of gaseous oxidized mercury species onto solid-phase sorbent traps, thermal desorption in the inlet of a modified APCI and detection using mass spectrometry; using this method, chemical species of oxidized mercury can be both identified and quantified.

Particulate-bound mercury (PBM) is trapped on to quartz and Teflon filters, which are acid digested, releasing dissolved species that are subsequently reduced to dissolved elemental mercury. Mercury is purged from the solution and measured by cold-vapor atomic fluorescence spectroscopy. Particulate-bound mercury is suspected to consist mostly of HgO, mercury(II) halides (HgX_2), elemental mercury, and mercury sulfide [19, 20]. As with KCl-coated denuders for measuring GOM, filters for measuring PBM can be influenced by artifacts. Gas-particle and particle-particle interactions on filters will increase over time and the latter increases with polydisperse particle populations [21].

Both GOM and PBM have shorter atmospheric residence times than GEM primarily due to higher wet and dry deposition. GOM is also more bioavailable to organic-mercury transforming bacteria in aqueous environments. The conversion of Hg^0 to GOM and interaction of Hg^0 to PBM is of prime importance to understanding the fate of mercury in our environment as both processes serve as important sinks [22]. Though particulate mercury concentrations are ultra-trace, PM_{10} is inhalable, $PM_{2.5}$ is respirable, and $PM_{1.0}$ can penetrate the pulmonary alveoli entering the bloodstream [20]. Understanding the contribution of particulate mercury is vital to understanding the ultimate risk of this bulk species to human and ecological health.

In this study, we use two methods for generating oxidized mercury aerosols: (a) vapor-phase condensation and (b) aqueous nebulization, and we characterize these aerosols using various optical and condensation-based particle sizers, high-resolution scanning transmission electron microscopy (HR-STEM), and particle interface preconcentration (designed for oxidized mercury) coupled soft ionization atmospheric pressure chemical ionization mass spectrometry (aka Hg mass spectrometry) analysis. A microcosm study was performed to evaluate the stability of the generated particles under near tropospheric conditions. We also determine the trapping efficiency of KCl-coated denuders (commonly used in GOM measurement) and particulate filters for three aerosolized oxidized mercury proxy species: $HgBr_2$, $HgCl_2$, and HgO. Various dry conditions (< 35% relative humidity) were used as the highest tropospheric reactive mercury (GOM + PBM) concentrations occur under those conditions [23], and flow rates through the denuder were varied from 1.0 to 10 L/min. The ability of PFA Teflon traps used in mercury mass spectrometry measurements were also assessed for trapping nanoparticulate mercury.

Materials and methods

Sub-micron and nanoparticulate oxidized mercury particles were formed from two methods: vapor-phase condensation and the nebulization of aqueous oxidized mercury species.

Formation of oxidized mercury aerosols—vapor-phase condensation

Anhydrous 10-mesh granules of 99.9999% purity $HgBr_2$ and $HgCl_2$ was obtained from Sigma-Aldrich, and ~ 0.5 g of HgX_2 granules were packed between two Teflon® frits (see Electronic Supplementary Material (ESM) Fig. S1) in $^3/_{64}$ in. O.D. and ¼ inch I.D. PFA Teflon® (Solon, OH). Sources were heated with heating tape connected to a temperature controller, which source temperature left to equilibrate over 10 min. A Big Hydrocarbon Trap from Agilent Technologies (Mississauga, ON) and PVDF filters from Parker Balston (Haverhill, MA) were used to scrub high purity nitrogen carrier gas produced by a Peak Scientific NM32LA Nitrogen Generator (Billerica, MA) of hydrocarbons and particles, respectively. An Omega low-flow inline heater was used to heat the nitrogen carrier gas, flowing at 0.25 L/min to the desired temperature; this flow was connected to a three-way valve and left to flow away from the source. Sources were equilibrated for 10 min at the desired source temperature between 25 and 50 °C before carrier gas of equivalent temperature was introduced to the source. As the vapor plume cooled in tubing downstream, oxidized mercury aerosols are formed.

Aerosol characterization process—high-resolution scanning transmission electron microscopy

Synthetic oxidized mercury aerosols were collected by the direct placement of STEM grids downstream from mercury halide sources purged with high purity N_2, through the use of an ESPnano 100 electrostatic precipitator (Spokane, WA) and in a microcosm experiment where STEM grids were placed 10 cm away from a watch glass holding 10-mesh $HgBr_2$ and $HgCl_2$ beads. The microcosm system was subjected to a 0.51 m/s linear flow rate of laboratory air, visible light exposure and kept at a pressure of ~ 740 Torr at 23 ± 2 °C for 1 week to mimic tropospheric conditions. 200 and 400 mesh Formvar/carbon-coated were obtained from Electron Microscope Sciences (Hatfield, PA) and SPI Supplies (West Chester, PA), respectively. An FEI Tecnai G^2 F20 kV Cryo-STEM with EDAX Octane T Ultra W/Apollo XLT_2 SDD and TEAM EDS Analysis System (Hillsboro, OR) was used to analyze samples.

Aerosol characterization process—aqueous suspensions

Particle concentrations and size distributions for synthetic $HgCl_2$ and $HgBr_2$ particles suspended in aqueous media, formed from vapor-phase condensation, with hydrodynamic radii of 30–2000 nm, were obtained using a Nanosight NS500 from Malvern Instruments (Ann Arbor, MI). Sources were equilibrated to a given temperature for 10 min before an N_2 carrier gas flow rate of 0.25 L/min was bubbled into 500 μL of 0.1 μm filtered milliQ water. This suspended aerosol solution was introduced to the Nanosight NS500. Nanoparticle tracking analysis (NTA) involves tracking the motion tracking of individual particles from scattered laser light and using the Stokes-Einstein equation to determine a hydrodynamic radius. Results obtained are the average concentration for ten replicates for each solution introduced.

Formation of mercury halide aerosols—aqueous nebulization and drying

30.1 mg of 99.999% trace metals basis $HgCl_2$ obtained from Sigma-Aldrich (St. Louis, MO) was dissolved with nanopure water into a 50.00 mL Pyrex No. 5460 volumetric flask. Similarly, 30.8 mg of 99.998% trace metals basis $HgBr_2$ and 31.3 mg of 99.0% ACS reagent HgO red obtained from Sigma-Aldrich (St. Louis, MO) to create 0.06% (w/v) solutions. Solutions were sonicated at 50 °C to promote dissolution. The aerosol formation process was adapted for the mercury sciences from [24] and depicted in Fig. 1. 0.06% (w/v) aqueous oxidized mercury solutions were loaded into 10 mL Luer Lock tip sterile polypropylene syringes from Terumo Corporation (Laguna, Philippines) and dispensed using a GenieTouch™ infusion dual syringe pump from Kent Scientific Corporation (Torrington, CT) at 10 μL/min. The solution entered a C-Flow 700d PFA Nebulizer from the Savillex Corporation (Minnetonka, MN) through platinum-cured, low-volatile grade, silicone tubing. Compressed air obtained from Praxair Canada (Mississauga, ON) scrubbed of particles using a Whatman HEPA-Cap 150 (Little Chalfont, Buckinghamshire, UK) was introduced to the nebulizer at 20 psi to create a consistent stream of aerosol.

Aerosol drying process—aerosol nebulization and drying

The aerosol stream entered a three-port in-house built mixing chamber where laboratory air was introduced through a HEPA filter to compensate for the flow rates required for the experiments. Following dilution, aerosol entered a cylindrical polycarbonate silica gel-based double diffusion dryer where water from the aerosol is removed. The relative humidity of the aerosol stream exiting the diffusion dryers was measured using an iCelsius Sentinel Next Temperature and Relative Humidity sensor from Aginova Inc. (Mason, OH). The humidity of the exiting aerosol stream was varied by removing diffusion dryers from the set-up.

KCl-coated denuders

A quartz annular denuder was rinsed and soaked with distilled water before cleaning with 10% reagent grade nitric acid,

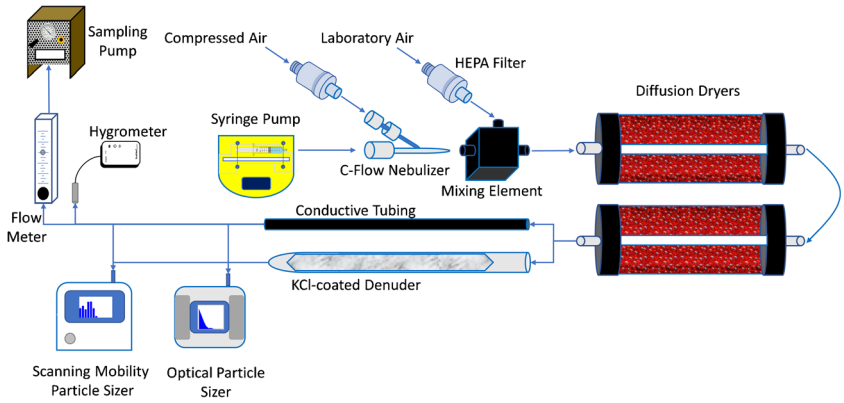

Fig. 1 Experimental set-up for oxidized mercury aerosol generation by aqueous nebulization and drying, KCl-coated denuder experiments and measurement by SMPS and OPS

nanopure water, and reagent grade methanol. The denuder was then dried in a mercury-free laminar fume hood. 14.5 g of potassium chloride was dissolved in 100 mL of water and drawn by vacuum into the vertically positioned quartz annular denuder clamped in place to a ring stand. The solution was drawn up to the active denuder surface, allowed to sit, and slowly drained for 1 min for each step, respectively. The process was repeated two more times. Reagent grade (68–70%) nitric acid and reagent grade methanol (98.8%) for cleaning the quartz annular denuder were obtained from ACP Chemical Inc. (Montreal, QC) and crystalline ACS grade potassium chloride (99.0–100.5%) for coating the denuder was purchased from Fisher Scientific Company (Ottawa, ON). The inlet of the denuder was wiped dry before the entire denuder was dried with mercury-free air produced using a Model 1100 zero air generator from Tekran Inc. (Toronto, ON). The KCl-coated denuder was thermally conditioned in a Thermolyne Sybron F-21125 tube furnace oven from ThemoFisher Scientific (Waltham, MA) at 525 °C for 1 h.

Denuder uptake experiments

The dry oxidized mercury aerosol entered either a KCl-coated denuder or conductive tubing of equal length from TSI Incorporated (Shoreview, MN) before being drawn into a particle sizing instruments. A NanoScan Scanning Mobility Particle Sizer (SMPS), Model 3910 from TSI Inc., was used to determine the aerosol particle size distributions from particles ranging in size from 10 to 420 nm across 12 bins with a 1 scan/min measurement rate and a sampling rate of 1 L/min. Scanning mobility particle sizing involves the addition of a charge to incoming sub-micron particles, selection of a given particle size using electric-mobility, and condensing the particle with isopropanol to detect using optical scattering resulting in discrete size-resolved nano- and sub-micron particle concentrations. An Optical Particle Sizer (OPS) Model 3310 from TSI Inc. was used to determine the aerosol particle size distributions for particles ranging in size from 300 nm to 10 μm across 16 bins with a 1 scan per 10-min measurement rate and a sampling rate of 0.7 L/min. A series of ten 1-min runs for the SMPS or one 10-min run for the OPS would be considered a "batch," with seven batches of uptake experiments conducted under either control and experimental conditions, and batch order pre-determined at random. Four flow rates were assessed for the uptake experiments including 1.0 L/min (from the sampling flow rate of the SMPS only), 1.7 L/min (from the combined sampling flow rates of the SMPS and OPS), 5 L/min and 10 L/min (achieved from the combining sampling flow rates of SMPS, OPS and a Vac-u-Go Air Sampler from SKC Incorporated (Eighty Four, PA)).

Particle trap preconcentration—mercury mass spectrometry

The detailed methodology for particle trap preconcentration coupled soft ionization mass spectrometry has been described by Deeds et al. [4]. Briefly, synthetic $HgBr_2$ and $HgCl_2$ aerosols were collected on particle traps consisting of a variety of sorbents including gold fiber, glass beads, silver granules, PFA Teflon, and polysulfide-coated copper-doped iron nanoparticles (ESM Fig. S2). Traps were housed in either ¼ inch O.D. glass or PFA Teflon tubing, with sorbent held in place using silanized glass wool or PFA Teflon frits. Exposure times for the traps to HgX_2 vapor-phase condensation aerosol generation flows varied from 5 s to 1 min, and the mercury(II) aqueous nebulization generation sources from 1 to 10 s. Traps were placed in a modified atmospheric pressure chemical ionization inlet, heated for 1.2 min at 200 °C, and desorbed using a 1 L/min 1% SF_6 in isobutane carrier gas. The Agilent 6140 single quadrupole mass spectrometer was optimized to the following set-points: corona current at 30 μA, capillary voltage to 750 V, N_2 drying gas flow rate and temperature at 5 L/min and heated to 200 °C, respectively, and fragmentor voltage to 90 V. $HgBr_2$, $HgCl_2$, and mercury(II) bromochloride (HgBrCl) were detected as fluoride complexes at m/z 287–295, 331–341, and 388–396, respectively. Other

mixed mercury(II) halides were also identified, such as $HgBr_2Cl$ and $HgCl_2Br$.

Aerosol density analysis

Average aerosol concentrations and standard deviations were determined for each particle size bin and compared between the conductive tubing control and KCl-coated denuder for the denuder uptake experiments. Analysis of variance (ANOVA) was performed using a 95% confidence interval over 70 samples to determine if the difference in means between the two conditions was statistically significant. The mean concentration of aerosol generated for a given particle size interval was subjected to a one-tailed *t* test to determine if the concentration showed a statistically significant difference from zero. OriginPro software from OriginLab Corporation (Northampton, MA) was used for all statistical analyses.

Results and discussion

Aerosol generation from oxidized mercury sources via vapor condensation

Higher concentrations of particles generated from vapor-phase condensation were detected by SMPS and OPS, with increasing source temperature and vapor concentration (Fig. 2a). Significant fluxes of mercury aerosols were consistently detected when sources were heated to 50 °C irrespective of source composition (ESM Fig. S3). As the vapor pressure of $HgBr_2$ and $HgCl_2$ increases with temperature, concentrations of these species in the gas stream induce solidification reactions at lower downstream temperatures producing mercury aerosols. The majority of particles were sub-micron sized (ESM Fig. S4). Mohadesi et al. use a similar principle to precipitate mercury(II) acetate nanostructures [25]. Exclusion of mercury uptake onto existing particles was achieved through HEPA filtration of the carrier gas upstream of the source. Aerosol occurrence at lower temperatures was also detected by the SMPS and OPS but limited by deposition losses onto the preceding tubing surface. Aerosol removal on the tubing downstream from the heated sources suggests possible perfluoroalkoxy Teflon surface catalyzed reactions and deposition induced by a declining temperature gradient [26].

Electron microscopy imaging of nanoparticulate oxidized mercury via HR-STEM-EDS

Synthetic mercury aerosols were collected using an electrostatic precipitator with TEM grids placed in line with the outflow from mercury vapor condensation sources heated from 25 to 50 °C. The EDS of selected particles confirmed the presence of both chlorine and bromine, providing evidence for mixed halide nanoparticle formation, suggesting that these particles did not dislodge from the solid HgX_2 granules

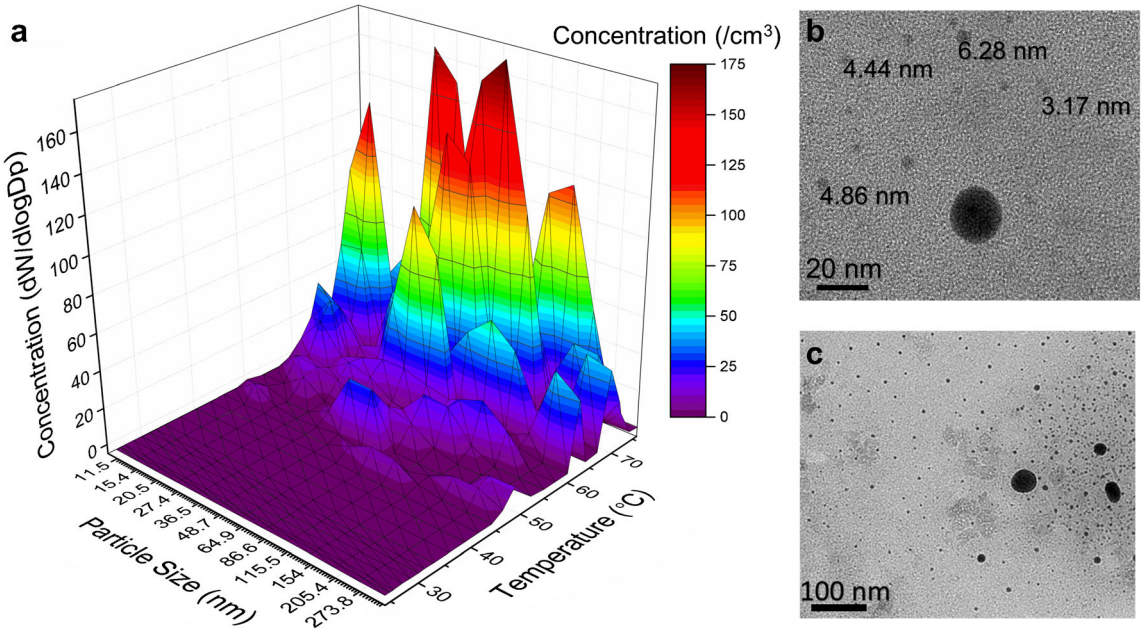

Fig. 2 **a** Particle size distribution surface for nanometer-sized mercury aerosols formed from a mixed 1:1 (by wt.) $HgCl_2$ and $HgBr_2$ source, where the majority of particles detected ranged between 50 and 175 nm in size. **b** High-resolution scanning transmission electron microscopy image of mercury aerosols from a mixed $HgCl_2$ and $HgBr_2$ source. HR-STEM can identify mercury aerosols which are smaller than the 10-nm diameter limit of the SMPS. **c** Transmission electron microscopy image of mercury aerosols from a mixed $HgCl_2$ and $HgBr_2$ source. The majority of the particles were between 3 and 100 nm in size

making up the sources themselves. Predominately spherical particles were observed with many smaller than (< 10 nm) what was capable of being detected by either the SMPS or through NTA (Fig. 2b, c). Few micron-sized particles were observed (ESM Fig. S5). While only a laboratory result, the existence of small mercury-containing nano-particulates below 10 nm has only just recently been observed in nature and would have significant implications on the fate of mercury [27]. Wet and dry deposition velocities of particulate-bound mercury decrease with particle size [28], allowing for longer transport distances. With decreased particle size, there is also a surface to volume ratio enhancement where surface chemistry can predominate [29]. Though the mechanisms for GOM and PBM deposition are different, as the diameter of particles decrease, they behave more like gases such as depositing through Brownian motion transport instead of gravitational settling [30]. The surface chemical and optical properties of nanoparticles also differ from larger particles and gaseous compounds, which has significance in radiative scattering, cloud condensation, and ultimately, in climate change [31].

Chemical speciation of mercury aerosols by particle trap preconcentration Hg-MS

A wide range of mercury-halogen species was observed when using the newly developed Hg-MS to characterize synthetic mercury aerosols, as shown in Fig. 3. These species included mixed halogen species and species containing multiple mercury atoms. Total ion counts increased with mercury source temperature consistent with the increased GOM vapor pressure and greater aerosol formation with temperature gradient–based condensation. The appearance of higher molecular weight species, including dimeric species, was readily observed for all sources and even at ambient temperatures though they are favored with increasing source temperature (ESM Fig. S6). Their presence may be indicative of fragmentation from mercury aerosols and not source ion reactions as they peak earlier in species evolution curves suggesting a combination of aerosol decomposition and ion source complex formation.

Particle stability and microcosm study

A borosilicate microcosm was constructed to examine potential transformation pathways of these particles and operated to mimic tropospheric conditions in which 10-mesh mercury halide beads were exposed to airflow for 1 week. Mercury aerosols were detected on charged TEM grids placed in the system, as shown in Fig. 4, showing the stability (size and crystallinity) of these particles in the air. These particles remained as condensed matter and were not immediately transformed to the gaseous phase, which is an essential feature of their potential role in the atmospheric processes such as residency and deposition rates. These particles also withstood the vacuum conditions present in the HR-STEM. A lack of mercury-containing tropospheric aerosol may then be attributable to deposition-based loses rather than gas-particle exchange losses [32].

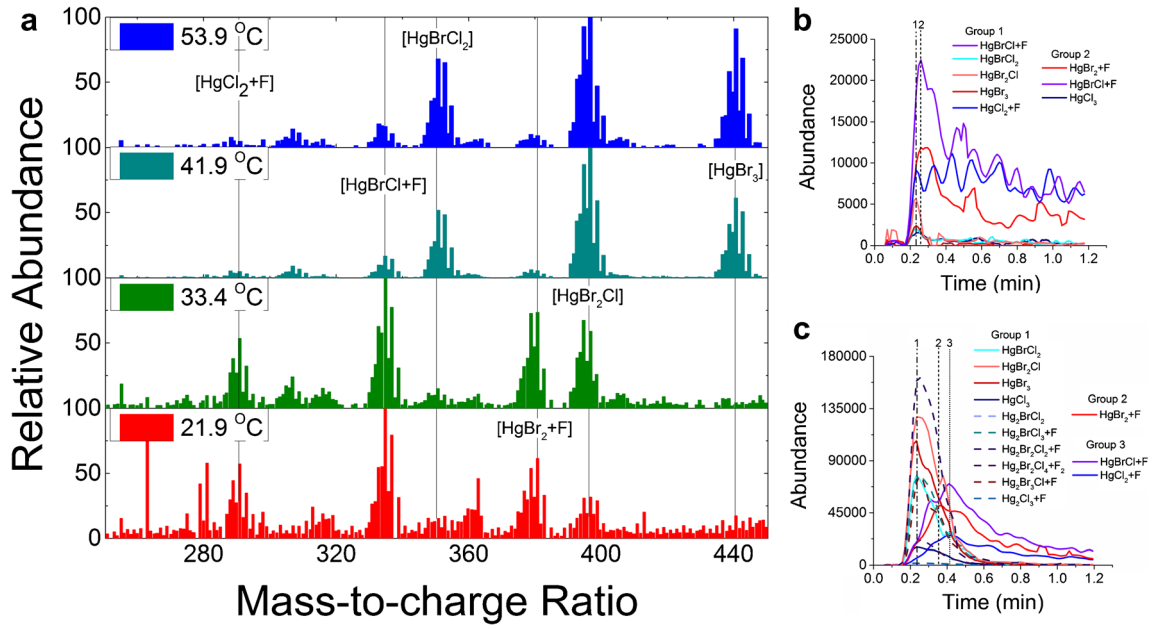

Fig. 3 **a** Mass spectra of mixed halogen species produced from heating sources between 20 and 50 °C. Species evolution curves for species produced by mixed 1:1 (by wt.) $HgCl_2$ and $HgBr_2$ at **b** 20 °C, at **c** 50 °C and trapped on PFA Teflon® traps following 1 min of 1 L/min UHP nitrogen flow

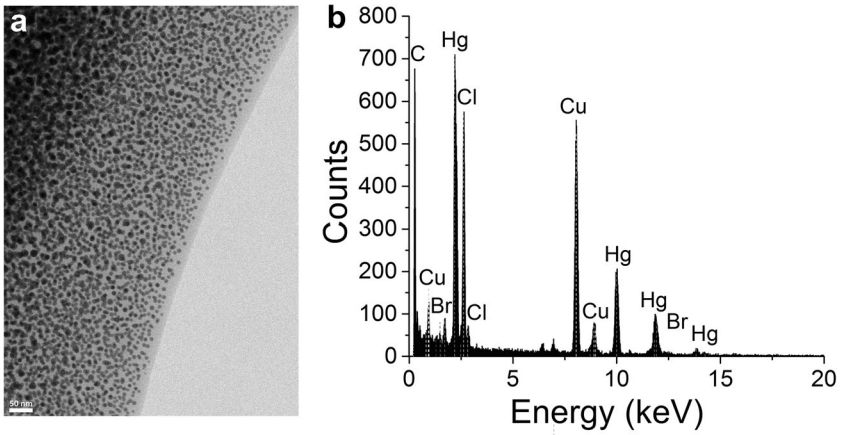

Fig. 4 **a** High-resolution transmission electron microscopy of mercury aerosols and **b** elemental analysis from energy-dispersive X-ray spectra of mercury nanoparticle. Image of mercury aerosols trapped on to a charged HR-TEM 400-mesh copper Formvar grid when exposed to $HgBr_2$ and $HgCl_2$ 10-mesh beads for a week under tropospheric conditions. The presence of mercury, chloride, and bromine is found in a single mercury ultrafine particle, suggesting that the particle is not a result of particles detaching from the beads and confirmation that mixed halogen species can form

Mercury particles in aqueous samples

Synthetic mercury nanoparticles were suspended in aqueous media to examine their fate and stability in aquatic environments. Nanoparticles are known to form aggregates in marine environments based on concentration, pH, ionic strength, and surface functionalization [31] and photoreactions of divalent mercury with thioglycolic acid and dissolved organic matter has been observed to produce crystalline and nanoscale HgS particles [31, 33, 34]. Though $HgBr_2$ and $HgCl_2$ are slightly soluble in water (0.017 mol/kg and 0.27 mol/kg, respectively) [35], sub-micron mercury particles were observed largely intact using NTA analysis (Fig. 5a). Particle sizes, based on the hydrodynamic radius, ranged from 20 to 350 nm, with the majority of particles between 75 and 250 nm, across a range of source compositions. Particles suspended from source tubing deposits, appearing downstream of the heated mercury source, showed slightly larger modes with fewer particles below 100 nm (Fig. 5b).

The formation of these particles under different carrier gas flow conditions may have influenced the resulting particle size distribution; aggregation and dissolution of particles in aqueous media may have also occurred. These latter processes are vital to the bioavailability of GOM species as they affect the surface area accessible for heterogeneous and biochemical reactions [31]. The distinct size distribution of suspended aerosols/deposits allows for the study of the chemistry of these aerosols in aqueous environments with surface functionalization by dissolved organics and inorganic ions that would change the breadth and maxima of the distributions [36]. Surface functionalization will also affect the solubility and release of dissolved oxidized mercury and the potential to enter mercury-methylating microorganisms [37]. Biota has also been shown to synthesize stable mercury(II) phosphate nanoparticles in the presence of $HgCl_2$ and identified for use in mercury remediation [38].

Aerosol generation from oxidized mercury solutions via aqueous nebulization

Generated aerosol counts were higher with aqueous nebulization than from vapor-phase condensation as the concentrations of oxidized mercury in nebulization solutions were orders of magnitude higher than the concentration of oxidized mercury vapor released. These generated nano- and sub-micron particle concentrations are shown in ESM Table S2. The solubilities of oxidized mercury vary across chemical speciation: HgX_2 are sparingly soluble, HgO is somewhat soluble, and mercury(II) nitrate is soluble [39]. Heating and sonication were used to promote the mechanical breakdown and dissolution of large particles.

Despite solubilities for species differing by orders of magnitude, the particle concentrations are similar across particle sizes with the highest concentrations of particles below 50 nm. Two separate HgO solutions produced comparable results showing the consistency of the aqueous nebulization aerosolization method. The concentrations of mercury(II) nitrate aerosols were significantly higher than those of mercury(II) halides and mercury(II) oxide; despite a high solubility, in dilute solutions, a basic insoluble mercury nitrate $Hg(OH)(NO_3)$ salt may form which may account for greater aerosol formation (Fig. 6). By increasing the draw of a downstream sampling pump, particle fluxes from the aqueous nebulization of $HgCl_2$ solutions were found to decrease with flow rate, by a factor of 10 (Fig. 7). The impact of humidity under relatively dry conditions on aerosol formation was statistically insignificant (ESM Fig. S9).

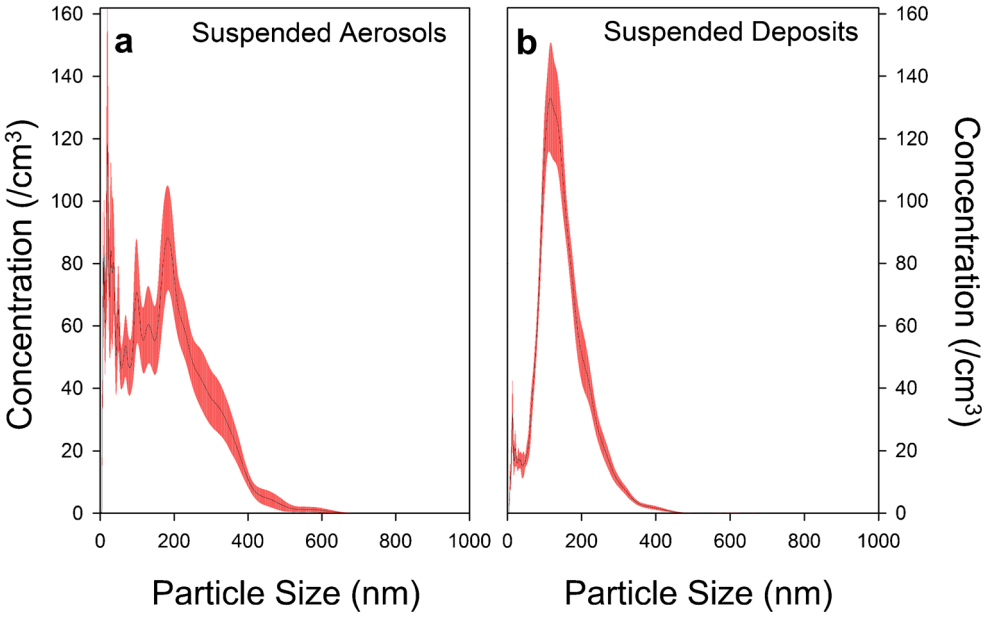

c

Suspension Source	Mean (n=10)	Mode (n=10)	Concentration (n=10)
$HgCl_2$ – 50 °C	144 nm ± 3.7 nm	134 nm ± 5.1 nm	1.52 x 10^8 /mL
$HgCl_2$ – Deposits	134 nm ± 3.1 nm	112 nm ± 5.6 nm	1.68 x 10^8 /mL
$HgBr_2$ – 50 °C	182 nm ± 11.8 nm	89 nm ± 18.1 nm	1.95 x 10^8 /mL
$HgBr_2$ – Deposits	176 nm ± 9.2 nm	143 nm ± 5.2 nm	0.58 x 10^8 /mL
Mixed – 50 °C	160 nm ± 18.9 nm	50 ± 17.3 nm	2.13 x 10^8 /mL
Mixed – Deposits	149 nm ± 3.4 nm	123 ± 5.3 nm	1.68 x 10^8 /mL

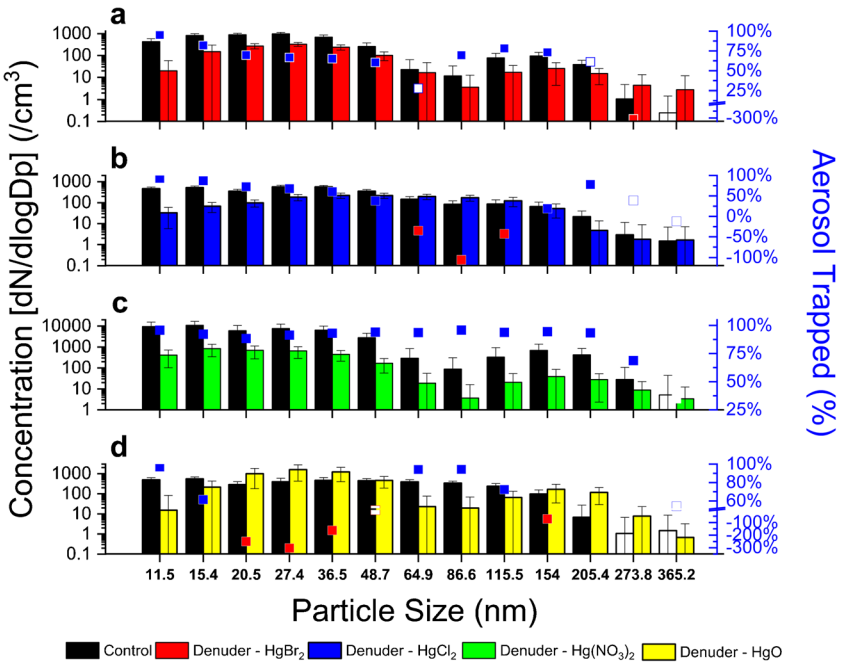

Fig. 5 Particle size distribution for **a** mercury aerosols and **b** tubing deposits suspended in aqueous media. The modes of particle sizes ranged between 80 and 200 nm from a mixed 1:1 (by wt.) $HgCl_2$ and $HgBr_2$ source immersed directly into milliQ water and for suspension mercury deposits heated to 50 °C with UHP nitrogen carrier gas flow of 0.25 L/min. Shown is the average of ten replicates with standard errors shown in red. Refer to ESM Figs. S7 and S8 for the impact of bromine and chlorine content on hydrodynamic particle size distributions

Fig. 6 The capture of various oxidized mercury species by KCl-coated denuder. The transmission of nanoparticulate mercury(II) halides, mercury(II) nitrate, and mercury(II) oxide through conductive tubing vs KCl-coated denuder at 5 L/min flow rate. Solid blue squares indicate the difference between conductive tubing and KCl-coated denuder was significant ($p > 0.05$); white squares with a blue outline indicate that the difference in transmission of aerosols through conductive tubing and the KCl-coated denuder was not significant ($p < 0.05$). Squares are colored red if the transmission of aerosols through the denuder was greater than through conductive tubing. Control bars are shaded white if there is no significant difference between the average mean of particles transmitted in comparison to zero ($p < 0.05$)

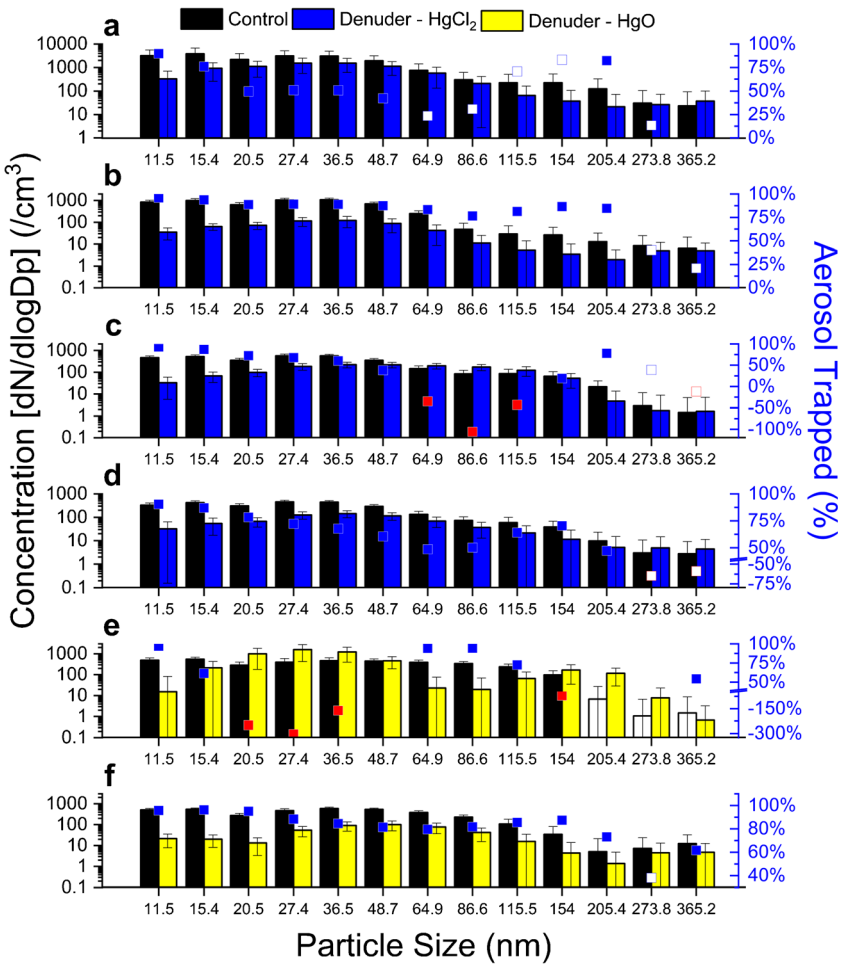

Fig. 7 The capture of mercury(II) oxide and mercury(II) chloride by KCl-coated denuder at varying flowrates. The trapping of nanoparticulate mercury(II) chloride at **a** 1 L/min, 5 L/min, and 15 L/min and mercury(II) oxide at 5 L/min and 1.5 L/min. The transmission of nanoparticulate mercury(II) chloride and mercury(II) oxide by through conductive tubing vs KCl-coated denuder at varying flowrates: **a** 1 L/min, **b** 1.7 L/min, **c**, **e** 5 L/min, and **d**, **f** 10 L/min. Solid blue squares indicate the difference between conductive tubing and KCl-coated denuder was significant ($p > 0.05$); white squares with a blue outline indicate that the difference in transmission of aerosols through conductive tubing and the KCl-coated denuder was not significant ($p < 0.05$). Squares are colored red if the transmission of aerosols through the denuder was greater than through conductive tubing. Control bars are shaded white if there is no significant difference between the average mean of particles transmitted in comparison to zero ($p < 0.05$)

Oxidized mercury nanoparticles particle capture by KCl-coated denuder

In comparing particle concentrations through a KCl-coated denuder and an equal length of conductive tubing, we see increasing particulate trapping on denuders for smaller diameter particles (Fig. 7). As seen in ESM Table S2, the mean particle counts for the largest sub-micron particles were often very low and at times, not significantly different from zero. In some cases, the particle counts for those highest sub-micron particles were often higher when aerosol stream passed through the denuder than through particle transmission-promoting conductive tubing. These instances may be caused either by particles dislodging from the KCl-coated denuder coating itself or due to coagulation of smaller nanoparticles through the experimental set-up.

At higher flow rates, the trapping of larger nanoparticles by the KCl-coated denuder was less effective, though surprisingly, we find significant transport of these larger sub-micron particles at 1 L/min flow rates. In terms of particulates, laminar flow is said to prevent small particles from impacting on the coating surface and cyclones and impactors remove larger particles upstream of the denuder [1]. A possible explanation is the flow was directed entirely to the SMPS instead of being teed-off to the OPS, or to the OPS and the sampling pump used to generate higher flow rates. With higher humidity, the transportation of particles through the denuder increases across all sizes (ESM Fig. S9).

Particulate penetration through membrane and syringe filters

Assessing a variety of filter types, the penetration of mercury nanoparticles through these filters was evaluated (ESM Fig. S10). Overall, quartz and Teflon filters which are routinely used in the mercury field provide the best capture of particulate mercury ($\sim 10^{-3}$% for 10 nm nanoparticles) while filters of larger pore sizes such as the QMA and qualitative filters allowed significant amounts of sub-micron particulates to pass ($\sim 10^{-1}$–10^{1}% for 10 nm nanoparticles). While it is expected that particles larger than the pore sizes of the filter would readily be captured, ultrafine particles, even those many times smaller than the pore size, will also have high deposition rates [30]. We expect the trapping curve, for particle size, to be

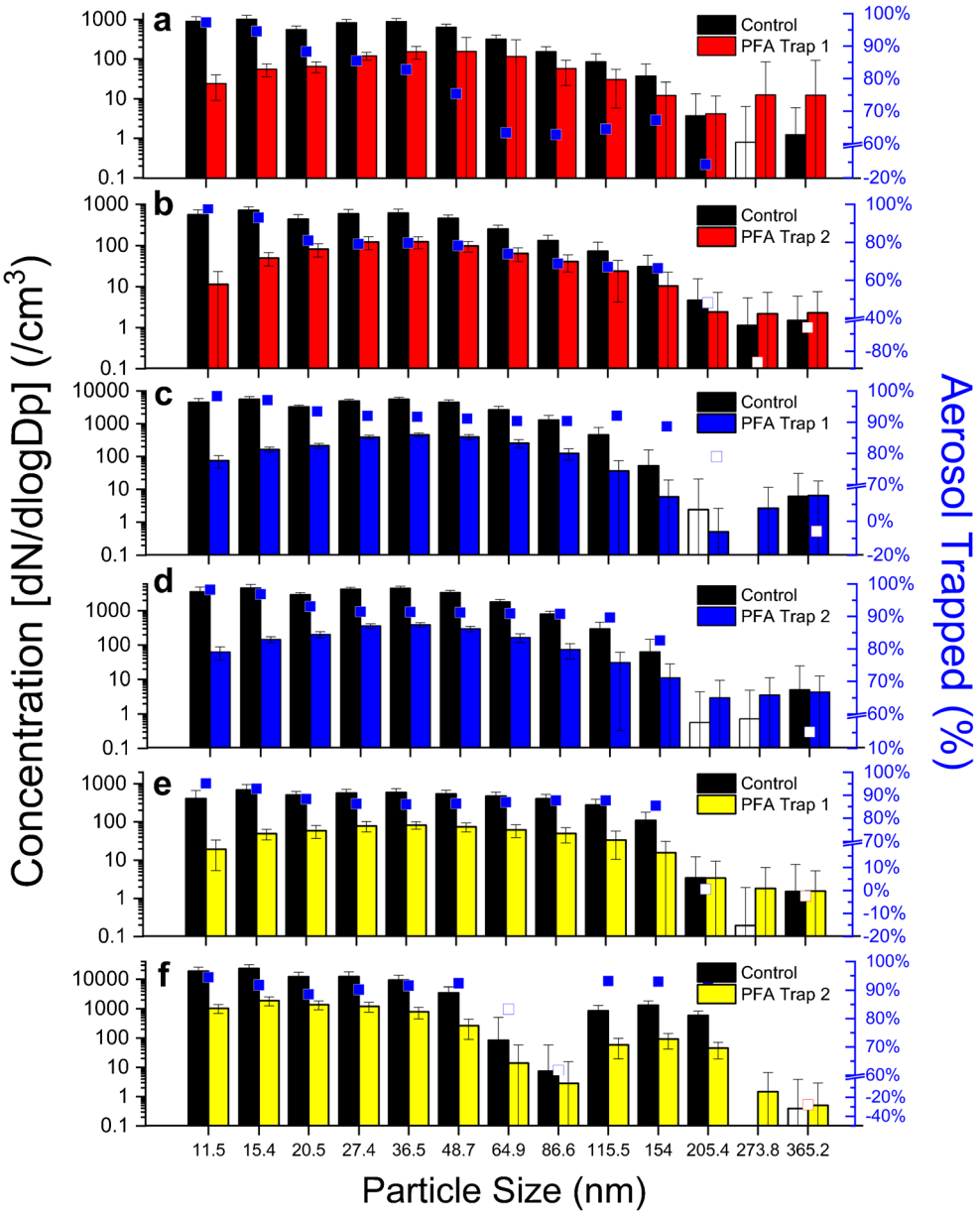

Fig. 8 The capture of various oxidized mercury species by PFA Teflon mercury mass spectrometry sorbent traps. The trapping of nanoparticulate mercury(II) halide and mercury(II) oxide on two (2) PFA Teflon Traps used in mercury mass spectrometry. The transmission of nanoparticulate mercury(II) halides and mercury(II) oxide by through conductive tubing vs PFA Teflon sorbent traps. Blue squares indicate the difference between conductive tubing and the PFA Teflon sorbent trap was significant ($p > 0.05$); white squares with a blue outline indicate that the difference in transmission of aerosols through conductive tubing and the PFA Teflon sorbent traps was not significant ($p < 0.05$). Squares are colored red if the transmission of aerosols was higher through the PFA Teflon sorbent trap

quadratic; thus, larger sub-micron particles of smaller diameters than the pore size will have the highest rates of breakthough.

Particle capture and speciation

As part of an emerging mercury mass spectrometry technique, the capacity for trapping oxidized mercury nanoparticles and sub-micron particles on nano- and microparticle sorbent traps used in the method is provided in Fig. 8. Nanoparticles are readily captured on these traps with efficiencies as high as 98% for the smallest nanoparticles. There is a definite size effect as particle capture efficiency decreases with size. For larger sub-micron particles, we see that the PFA sorbent trap may provide surfaces for smaller nanoparticles to coagulate to form larger particles. The particulate counts for these larger-sized sub-micron particles tend to be orders of magnitude lower with high variability and thus, some results are not statistically significant. For trapping and measuring nanoparticulate mercury, across species, the technique succeeds in capturing from 60 to > 95% of nanoparticles. The first detection of atmospheric gaseous $HgCl_2$ and $HgBr_2$ was observed using the techique in Montreal's urban air [4], and the low vapor pressure of species such as HgO supports condensation even at part per trillion concentrations [22]. Most recently, the detection of nanoparticulate mercury was confirmed in the Montreal's urban air [27].

Conclusions

In conclusion, aqueous nebulization and vapor-phase condensation methods were developed to produce steady and reproducible distributions of mercury nanoparticles and sub-micron particles. These nanoparticles have been characterized using scanning mobility and optical particle sizing, microscopy, and nano-tracking analysis and shown to be stable under tropospheric and aqueous conditions. Using mercury mass spectrometry, the chemical species present in these nanoparticles was assessed. Under the high temperatures of the ion source, these particles desorb HgX_2, which are readily measured. We also show the formation of mixed halide nanoparticles using HR-STEM. Finally, the interference of KCl-coated denuder measurements of GOM by mercury halide nanoparticles is confirmed across a range of experimental conditions and as high as 95% for the smallest nanoparticles (10 nm). The efficiency of particulate filters and nano- and micro-particulate sorbent filters and mercury mass spectrometry sorbent traps for capturing nanoparticulate mercury is also observed.

Acknowledgments The authors thank Dr. Hojatollah Vali and David Liu of the Facility for Electron Microscopy Research and also acknowledge Dr. Janusz Rak and Laura Montermini at the Montreal Children's Hospital for the use of the Nanosight NS500.

Funding information

This study received financial support from the Natural Sciences and Engineering Research Council of Canada (NSERC), the Canadian Foundation for Innovation (CFI), Le Fonds de recherche du Québec – Nature et technologies (FRQNT), Environment and Climate Change Canada, McGill University, and the Walter C. Sumner Foundation.

Compliance with ethical standards

Conflict of interest The authors declare that they have no conflicts of interest

References

1. Malcolm EG, Ford AC, Redding TA, Richardson MC, Strain BM, Tetzner SW. Experimental investigation of the scavenging of gaseous mercury by sea salt aerosol. J Atmos Chem. 2010;63(3):221–34. https://doi.org/10.1007/s10874-010-9165-y.
2. Denis MS, Song X, Lu JY, Feng X. Atmospheric gaseous elemental mercury in downtown Toronto. Atmos Environ. 2006;40(21):4016–24. https://doi.org/10.1016/j.atmosenv.2005.07.078.
3. Cairns E, Tharumakulasingam K, Athar M, Yousaf M, Cheng I, Huang Y, et al. Source, concentration, and distribution of elemental mercury in the atmosphere in Toronto, Canada. Environ Pollut. 2011;159(8–9):2003–8. https://doi.org/10.1016/j.envpol.2010.12.006.
4. Deeds DA, Ghoshdastidar A, Raofie F, Guerette EA, Tessier A, Ariya PA. Development of a particle-trap preconcentration-soft ionization mass spectrometric technique for the quantification of mercury halides in air. Anal Chem. 2015;87(10):5109–16. https://doi.org/10.1021/ac504545w.
5. Seo Y-S, Han Y-J, Choi H-D, Holsen TM, Yi S-M. Characteristics of total mercury (TM) wet deposition: scavenging of atmospheric mercury species. Atmos Environ. 2012;49:69–76. https://doi.org/10.1016/j.atmosenv.2011.12.031.
6. Xiao Z, Sommar J, Wei S, Lindqvist O. Sampling and determination of gas phase divalent mercury in the air using a KCl coated denuder. Fresen J Anal Chem. 1997;358(3):386–91. https://doi.org/10.1007/s002160050434.
7. McClure CD, Jaffe DA, Edgerton ES. Evaluation of the KCl denuder method for gaseous oxidized mercury using HgBr2 at an in-service AMNet site. Environ Sci Technol. 2014;48(19):11437–44. https://doi.org/10.1021/es502545k.
8. Lyman SN, Jaffe DA, Gustin MS. Release of mercury halides from KCl denuders in the presence of ozone. Atmos Chem Phys. 2010;10(17):8197–204. https://doi.org/10.5194/acp-10-8197-2010.
9. Huang JY, Miller MB, Weiss-Penzias P, Gustin MS. Comparison of gaseous oxidized Hg measured by KCl-coated denuders, and nylon and cation exchange membranes. Environ Sci Technol. 2013;47(13):7307–16. https://doi.org/10.1021/es4012349.
10. Landis MS, Stevens RK, Schaedlich F, Prestbo EM. Development and characterization of an annular denuder methodology for the measurement of divalent inorganic reactive gaseous mercury in ambient air. Environ Sci Technol. 2002;36(13):3000–9. https://doi.org/10.1021/es015887t.
11. Lynam MM, Keeler GJ. Artifacts associated with the measurement of particulate mercury in an urban environment: the influence of elevated ozone concentrations. Atmos Environ. 2005;39(17):3081–8. https://doi.org/10.1016/j.atmosenv.2005.01.036.
12. Pal B, Ariya PA. Studies of ozone initiated reactions of gaseous mercury: kinetics, product studies, and atmospheric implications. Phys Chem Chem Phys. 2004;6(3):572–9.
13. Pal B, Ariya PA. Gas-phase HO•-initiated reactions of elemental mercury: kinetics, product studies, and atmospheric implications. Environ Sci Technol. 2004;38(21):5555–66. https://doi.org/10.1021/es0494353.
14. Ariya PA, Khalizov A, Gidas A. Reactions of gaseous mercury with atomic and molecular halogens: kinetics, product studies, and atmospheric implications. J Phys Chem A. 2002;106(32):7310–20. https://doi.org/10.1021/jp020719o.
15. Gustin M, Jaffe D. Reducing the uncertainty in measurement and understanding of mercury in the atmosphere. Environ Sci Technol. 2010;44(7):2222–7. https://doi.org/10.1021/es902736k.
16. Yang H (2002) Effects of fly ash on the oxidation of mercury during post-combustion conditions.
17. Kos G, Ryzhkov A, Dastoor A, Narayan J, Steffen A, Ariya PA, et al. Evaluation of discrepancy between measured and modelled oxidized mercury species. Atmos Chem Phys. 2013;13(9):4839–63. https://doi.org/10.5194/acp-13-4839-2013.
18. Raofie F, Ariya PA. Product study of the gas-phase BrO-initiated oxidation of Hg0: evidence for stable Hg1+ compounds. Environ Sci Technol. 2004;38(16):4319–26.
19. Feng XB, Lu JY, Gregoire DC, Hao YJ, Banic CM, Schroeder WH. Analysis of inorganic mercury species associated with airborne particulate matter/aerosols: method development. Anal Bioanal Chem. 2004;380(4):683–9. https://doi.org/10.1007/s00216-004-2803-y.
20. Pyta H, Rogula-Kozlowska W. Determination of mercury in size-segregated ambient particulate matter using CVAAS. Microchem J. 2016;124:76–81. https://doi.org/10.1016/j.microc.2015.08.001.
21. Malcolm EG, Keeler GJ. Evidence for a sampling artifact for particulate-phase mercury in the marine atmosphere. Atmos Environ. 2007;41(16):3352–9. https://doi.org/10.1016/j.atmosenv.2006.12.024.
22. Murphy DM, Thomson DS, Mahoney MJ. In situ measurements of organics, meteoritic material, mercury, and other elements in aerosols at 5 to 19 kilometers. Science. 1998;282(5394):1664–9. https://doi.org/10.1126/science.282.5394.1664.

23. Marusczak N, Sonke JE, Fu X, Jiskra M. Tropospheric GOM at the pic du Midi observatory-correcting bias in denuder based observations. Environ Sci Technol. 2016. https://doi.org/10.1021/acs.est.6b04999.
24. Nazarenko Y, Rangel-Alvarado RB, Kos G, Kurien U, Ariya PA. Novel aerosol analysis approach for characterization of nanoparticulate matter in snow. Environ Sci Pollut Res. 2016:1–14. https://doi.org/10.1007/s11356-016-8199-3.
25. Mohadesi A, Ranjbar M, Hosseinpour-Mashkani SM. Solvent-free synthesis of mercury oxide nanoparticles by a simple thermal decomposition method. Superlattice Microst. 2014;66:48–53. https://doi.org/10.1016/j.spmi.2013.11.017.
26. Liu J, Pui DYH, Wang J. Removal of airborne nanoparticles by membrane coated filters. Sci Total Environ. 2011;409(22):4868–74. https://doi.org/10.1016/j.scitotenv.2011.08.011.
27. Ghoshdastidar AJ, Ariya PA. The existence of airborne mercury nanoparticles. Sci Rep-Uk. 2019;9(1):10733. https://doi.org/10.1038/s41598-019-47086-8.
28. Jen YH, Chen WH, Yuan CS, Ie IR, Hung CH. Seasonal variation and spatial distribution of atmospheric mercury and its gas-particulate partition in the vicinity of a semiconductor manufacturing complex. Environ Sci Pollut Res. 2014;21(8):5474–83. https://doi.org/10.1007/s11356-013-2441-z.
29. Subir M, Ariya PA, Dastoor AP. A review of the sources of uncertainties in atmospheric mercury modeling II. Mercury surface and heterogeneous chemistry - a missing link. Atmos Environ. 2012;46:1–10. https://doi.org/10.1016/j.atmosenv.2011.07.047.
30. Seinfeld JH, Pandis SN. Atmospheric chemistry and physics: from air pollution to climate change: John Wiley & Sons; 2012.
31. Grassian VH. When size really matters: size-dependent properties and surface chemistry of metal and metal oxide nanoparticles in gas and liquid phase environments†. J Phys Chem C. 2008;112(47):18303–13. https://doi.org/10.1021/jp806073t.
32. Murphy DM, Hudson PK, Thomson DS, Sheridan PJ, Wilson JC. Observations of mercury-containing aerosols. Environ Sci Technol. 2006;40(10):3163–7. https://doi.org/10.1021/es052385x.
33. Si L, Ariya PA. Photochemical reactions of divalent mercury with thioglycolic acid: formation of mercuric sulfide particles. Chemosphere. 2015;119:467–72. https://doi.org/10.1016/j.chemosphere.2014.07.022.
34. Pham AL-T, Morris A, Zhang T, Ticknor J, Levard C, Hsu-Kim H. Precipitation of nanoscale mercuric sulfides in the presence of natural organic matter: structural properties, aggregation, and biotransformation. Geochim Cosmochim Acta. 2014;133(0):204–15. https://doi.org/10.1016/j.gca.2014.02.027.
35. Ariya PA, Amyot M, Dastoor A, Deeds D, Feinberg A, Kos G, et al. Mercury physicochemical and biogeochemical transformation in the atmosphere and at atmospheric interfaces: a review and future directions. Chem Rev. 2015;115(10):3760–802. https://doi.org/10.1021/cr500667e.
36. Mwilu SK, El Badawy AM, Bradham K, Nelson C, Thomas D, Scheckel KG, et al. Changes in silver nanoparticles exposed to human synthetic stomach fluid: effects of particle size and surface chemistry. Sci Total Environ. 2013;447(0):90–8. https://doi.org/10.1016/j.scitotenv.2012.12.036.
37. Mazrui Nashaat M, Seelen E, King'ondu CK, Thota S, Awino J, Rouge J, et al. The precipitation, growth and stability of mercury sulfide nanoparticles formed in the presence of marine dissolved organic matter. Environ Sci Process Impacts. 2018;20(4):642–56. https://doi.org/10.1039/C7EM00593H.
38. Sinha A, Khare SK. Mercury bioaccumulation and simultaneous nanoparticle synthesis by Enterobacter sp. cells. Bioresour Technol. 2011;102(5):4281–4. https://doi.org/10.1016/j.biortech.2010.12.040.
39. Clever HL, Johnson SA, Derrick ME. The solubility of mercury and some sparingly soluble mercury salts in water and aqueous electrolyte solutions. J Phys Chem Ref Data. 1985;14(3):631–80. https://doi.org/10.1063/1.555732.